

DETC2020-22246

HYBRID SOFT-RIGID DEPLOYABLE STRUCTURE INSPIRED BY THICK-PANEL ORIGAMI

Chenyang Liu, Perla Maiolino, Yunfang Yang and Zhong You¹

Department of Engineering Science
University of Oxford
Oxford OX1 3PJ, U.K.

Email: {chenyang.liu, perla.maiolino, yunfang.yang, zhong.you}@eng.ox.ac.uk

ABSTRACT

Recently, the techniques of origami have become the subject of scientific research. Such methods of folding plates are suitable for practical engineering applications. This paper proposes a novel structure, inspired by thick-panel origami, with hybrid rigid bodies and flexible hinges. Able to be expanded, flipped, and rotated, the waterbomb origami pattern has been chosen to produce a large number of configurations. The mechanism and motion analysis of a single unit and its basic assembly are conducted theoretically and also simulated. An additive fabrication method based on 3D printing makes it a one-step process to achieve a balance between rigidity and flexibility in the structure. Different configurations are demonstrated in three assemblies that exhibit good transformability, reconfigurability, and scalability. With the expansion/packaging ratio ranging from 0.11 to 7.2 in a modular unit, a mechanical metamaterial of negative Poisson's ratio can be obtained at any spatial size. In addition, our design's potential for robotic applications is also validated by an adaptable gripper with tendon-driven systems.

1. INTRODUCTION

First known as the traditional Japanese art of paper folding, origami can have rigid panels or facets but is flexible along creases, allowing people to construct 3D models from 2D plane materials [1]. The folding principles lead to a set of predictable motions capable of large-scale shape deformation, which has the potential to exhibit soft-bodied properties. This makes origami-inspired structures useful for engineering applications,

examples of which include mechanical metamaterials [2], soft robotics [3], and deployable solar panels [4].

Previous examples of origami applications were usually built from flat sheets of paper or polymer, where thickness was not taken into consideration. Despite the potential shown by the prototypes, an obvious limitation is that thin materials are relatively fragile and prone to fatigue from repeated folding and unfolding [5]. It was necessary to develop reliable and robust structures for industrial use.

Folding rigid thick panels to create origami structures could be an alternative. Four-, five-, and six-crease single-vertex origamis of thick panels, which can produce identical motions to zero-thickness origami, were first reported in [6]. Later, the waterbomb origami based on thick panels was further analysed for tessellation [7]. In addition to being controlled more easily because of the reduced number of degrees of freedom (DOF) [6], the thick-panel origami can also be more durable due to the non-zero thickness plate. So far, however, only a few studies have been conducted on the mechanism of the thick-panel waterbomb and its tessellations. More configurations and applicable fabrication methods should be explored.

In this paper, we report the design of a foldable structure inspired by the thick-panel origami, where the thickness change allows for reliable rigid bodies and flexible hinges at the same time. The six-crease waterbomb pattern is used to produce different motions: expanding, right-flipping, left-flipping, and rotating motions from the unfolded state. In fabrication, to

¹ Address all correspondence to this author.

achieve a balance between durability and flexibility, 3D printing with thermoplastic polyurethane (TPU) material has been adopted to create parts of variable thicknesses to work as bodies or hinges. The proposed structure, as a modular unit, can be assembled to any size, thus producing a series of transformable configurations. Such deployable structures show the potential for metamaterial and robotic applications.

The paper is organized as follows. We start with the mechanism and folding principles of the thick-panel waterbomb. The motion trajectories of a single unit and the transformable configurations of a basic assembly are analysed in detail. Then, a fabrication method to design hybrid structures with rigid bodies and flexible hinges is proposed. Based on this, we test our design in three assemblies to show their reconfigurability and scalability. We further demonstrate the structure’s potential by illustrating a proof-of-concept case study on a tendon-driven gripper. Conclusions and future work are given at the end of the paper.

2. ORIGAMI DESIGN

Several origami patterns, including the waterbomb base, Yoshimura pattern, diagonal pattern and Miura-ori pattern, have been used to develop practical applications [8-13]. We begin with a six-crease square waterbomb pattern to create reconfigurable structures, which is also applicable to other shapes. In this section, the principles of the thick-panel waterbomb will be first introduced, and then we will focus on structure design, motion analysis and transformable configurations of both the single unit and its basic assembly.

2.1 Thick-Panel Waterbomb Origami Pattern

With the capability to expand and contract in all directions, the waterbomb origami can constitute structures to produce a variety of predictable motions.

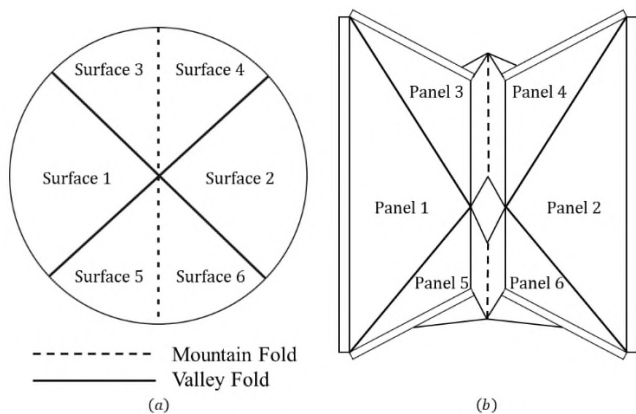


FIGURE 1: Waterbomb origami. (a) Six-crease waterbomb base; (b) its semi-folded counterpart based on thick panels.

A typical six-crease waterbomb base is displayed in Fig. 1(a). To create the waterbomb of non-zero thickness, our approach is to put hinges at the top or the bottom of flat thick panels to replace the mountain or valley folds of paper-based origami. Then a thick-panel model can be obtained as in Fig. 1(b).

2.2 Mechanism and Motion Trajectory Analysis

Consider the six-crease thick-panel waterbomb in Fig. 2. The folding lines have been rotated by 45° anticlockwise in comparison with the pattern in Fig. 1, and the valley folds are orthogonal to each other. The model consists of two cuboids and four triangular prisms connected in a loop. They congruent with each other respectively, thus bringing great symmetric properties to the model. The assembly exhibits some unique kinematic features, which are shown in Fig. 3.

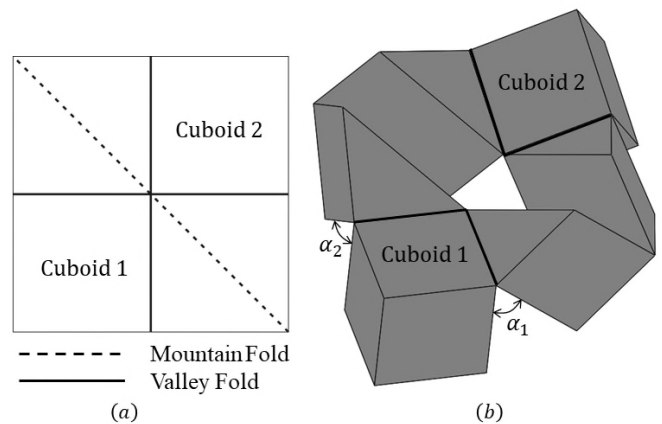


FIGURE 2: Square-based waterbomb origami pattern and its 3D structure. (a) Top view of completely-unfolded model; (b) 3D model in its partially-expanded state.

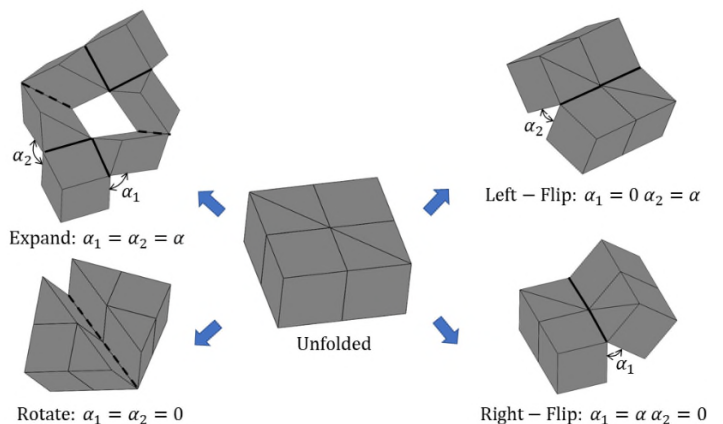


FIGURE 3: Expanding, flipping, and rotating motions generated from unfolded thick-panel waterbomb.

In Fig. 3, Cuboid 1 is a fixed base while α_1 and α_2 are input angles. In the folding process, the change of input angles alters the positions of the two prisms connected to Cuboid 1 and finally leads to the movement of Cuboid 2. Thus, we define hinges and prisms that trigger motions as active parts while the others are passive. The active hinges are highlighted with solid or dotted lines. The initial unfolded model with zero input angles is at the bifurcation point. With different operations of α_1 and α_2 , we can obtain four main folding motions: expand, right-flip, left-flip, and rotate. In the expanding motion, the model is an overconstrained structure with single DOF.

Clearly, the rotating motion, together with two flipping motions, can create a circular trajectory for Cuboid 2. What we need to analyse is what motion path Cuboid 2 can achieve while experiencing the expanding motion. In Fig. 4, a spatial rectangular coordinate system is established with Cuboid 1 as the base. The parameters are described in Table 1.

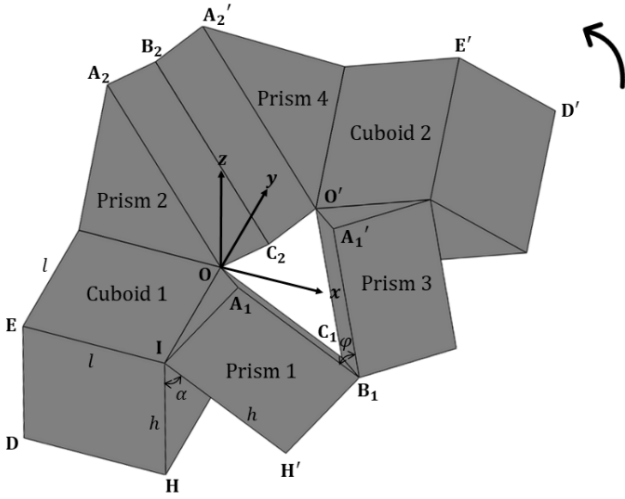


FIGURE 4: Schematic model in semi-expanded state and corresponding spatial rectangular coordinate system.

TABLE 1: Parameter set-up

Parameter	Physical meaning
l	Length of cuboids and prisms' base
h	Height of cuboids and prisms
α	Input angle, dihedral angle between Plane OIH and Plane OIH'
φ	Output angle, dihedral angle between Plane $OC_1B_1A_1$ and Plane $O'C_1B_1A_1'$

To simplify, take l as 1. We use Cuboid 2's centroid, the midpoint of $O'D'$, to represent its trajectory.

The symmetric properties make $B_1, C_1, B_2,$ and C_2 on the same plane and divide φ into two equal angles, one of which is the dihedral angle between Plane $OA_1B_1C_1$ and Plane $B_1C_1B_2C_2$. Two normal vectors of the two planes are

$$\vec{N}_1 = \left(1, 1, \frac{1-\cos \alpha}{\sin \alpha}\right) \quad (1)$$

$$\vec{N}_2 = \left(1, \frac{1}{\cos \alpha}, \tan \alpha\right) \quad (2)$$

Therefore, φ can be obtained from

$$\cos \frac{\varphi}{2} = \frac{|\vec{N}_1 \cdot \vec{N}_2|}{|\vec{N}_1| |\vec{N}_2|} = \frac{\sqrt{2} \sin \alpha}{\sqrt{(3+\cos \alpha)(1-\cos \alpha)}} \quad (3)$$

which yields

$$\varphi = 2 \cos^{-1} \left(\frac{\sqrt{2} \sin \alpha}{\sqrt{(3+\cos \alpha)(1-\cos \alpha)}} \right) \quad (4)$$

It is clear that h exerts no influence on the value of φ , and thus, we also assume $h = l = 1$.

Figure 5 shows the relationship between the input angle α and the output angle φ from both theoretical calculation and simulation in SolidWorks, which are mutually validated.

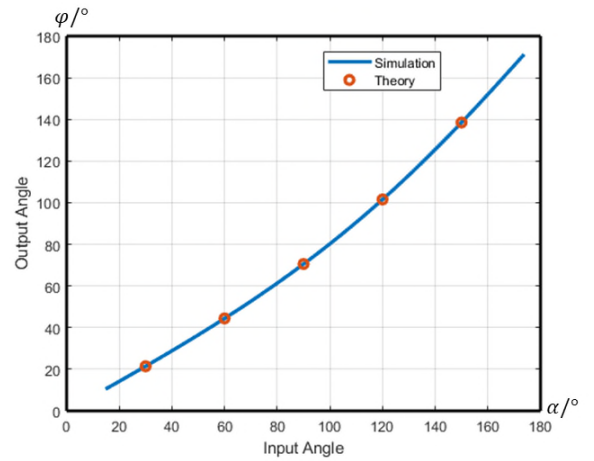


FIGURE 5: Relationship between output angle φ and input angle α .

The next step is to calculate the trajectory of O' . Due to symmetry, the coordinate of O' could be assumed as $(x_{O'}, y_{O'}, z_{O'})$, where $x_{O'} = y_{O'}$.

The geometrical conditions of O' are

$$\angle O'C_1O = \varphi \quad (5)$$

$$\vec{O'C_1} \cdot \vec{B_1C_1} = 0 \quad (6)$$

Then we can have the coordinate of O' below.

$$O' = \left(\frac{2 \sin \alpha}{3+\cos \alpha}, \frac{2 \sin \alpha}{3+\cos \alpha}, \frac{2(1-\cos \alpha)}{3+\cos \alpha} \right) \quad (7)$$

O' and D' only move on Plane OED . To understand their trajectories more straightforwardly, we use the cross-sectional view of the model by slicing it across a plane formed by Plane OED for further analysis. The new coordinate system is displayed in Fig. 6, where axis z remains the same as before whilst x' lies bisecting x and y .

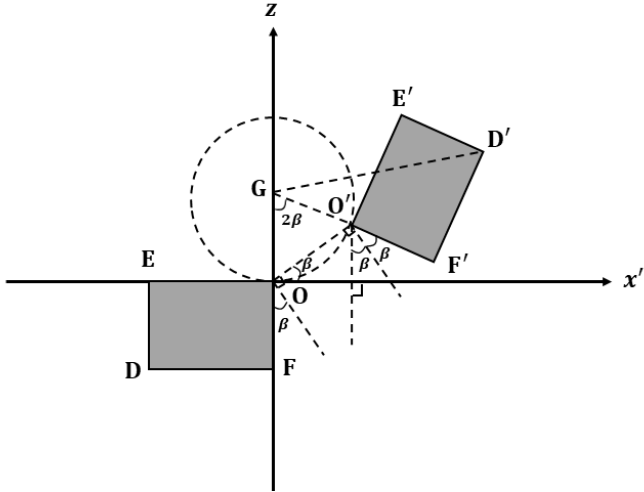


FIGURE 6: Cross-sectional view of semi-expanded model and corresponding planar coordinate system.

In Fig. 6, O' can be represented as

$$|\overline{OO'}| = 2 \sin \beta \quad (8)$$

where β is the angle between $\overline{OO'}$ and Plane xOy in the previous coordinate system. It indicates that the trajectory of O' is part of a circle with the centre point at $G(0, 1)$. The relationship between α and β is described as

$$\tan \beta = \frac{1 - \cos \alpha}{\sqrt{2} \sin \alpha} \quad (9)$$

Furthermore, it can be demonstrated that the three points G, O', F' are on the same line. Now it is safe to say that the trajectories of D', E' , and F' are all part of a circle with the same centre point $G(0, 1)$. The coordinate of D' is

$$x_{D'} = y_{D'} = \sqrt{2} \sin 2\beta + \cos 2\beta \quad (10)$$

$$z_{D'} = 1 + \sqrt{2} \sin 2\beta - 2 \cos 2\beta \quad (11)$$

where $\sin 2\beta = \frac{2\sqrt{2} \sin \alpha}{3 + \cos \alpha}$ and $\cos 2\beta = \frac{1 + 3 \cos \alpha}{3 + \cos \alpha}$. Then we can obtain the coordinate of centroid for Cuboid 2 as

$$x_{C_2} = y_{C_2} = \frac{3 \sin \alpha + \frac{3}{2} \cos \alpha + \frac{1}{2}}{3 + \cos \alpha} \quad (12)$$

$$z_{C_2} = \frac{2 \sin \alpha - \frac{7}{2} \cos \alpha + \frac{3}{2}}{3 + \cos \alpha} \quad (13)$$

2.3 Transformable Configurations of Basic Assembly

The inbuilt symmetricity enables single units to be assembled with each other. Figure 7 shows the basic assembly of four identical single units. The structure can achieve the same motions as a single unit, which is able to expand, flip, and rotate separately. In addition, the assembly can be synchronically operated to expand after the bifurcation point, as every two adjacent units share the same active part. The process is illustrated in Fig. 7, where the assembly starts from an unfolded state, then becomes patulous and finally ends with an expanded structure.

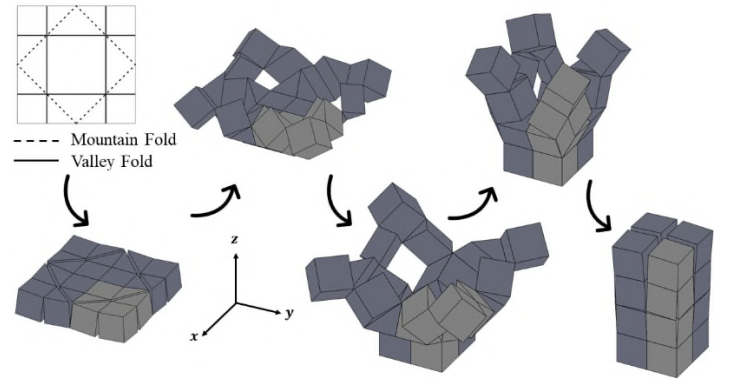


FIGURE 7: Basic assembly of four single units. The upper left picture shows folding pattern of the model and others are 3D structures in synchronically-expanded process.

The assembly's expansion/packaging ratio can be estimated by the area change in different directions. Usually the wider range of ratio means the higher potential to deform. We use the vertices of Cuboid 1 and the centroids of Cuboid 2 on two adjacent single units to represent the profile of the structure along axis x and y . The centroids of Cuboid 2 on each unit are used to shape the profile along axis z . Both profiles are shown in Fig. 8.

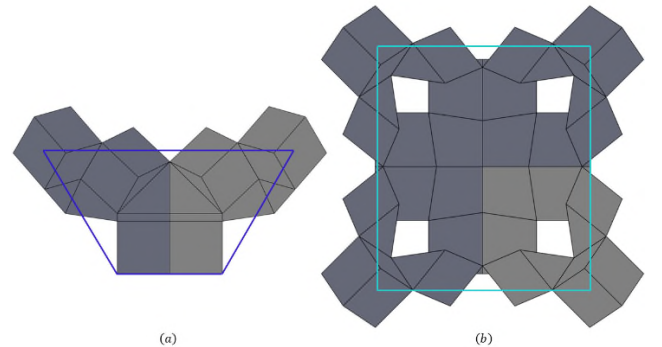


FIGURE 8: Side view and top view of semi-expanded basic assembly. (a) Estimated area along axis x and y included by purple line; (b) estimated area along axis z included by green line.

The area of each profile can be obtained from

$$S_{x/y} = (x_{c_2} + 2)(z_{c_2} + 1) \quad (14)$$

$$S_z = 4(x_{c_2} + 1)^2 \quad (15)$$

Here we define the expansion/packaging ratio as the current area divided by the initial area, of which the input angle is zero. Thus, the expansion/packaging ratio t is

$$t_{x/y} = \frac{S_{x/y}}{S_{x/y_0}} = \frac{4\left(3 \sin \alpha + \frac{7}{2} \cos \alpha + \frac{13}{2}\right)\left(2 \sin \alpha - \frac{5}{2} \cos \alpha + \frac{9}{2}\right)}{5(3 + \cos \alpha)^2} \quad (16)$$

$$t_z = \frac{S_z}{S_{z_0}} = \frac{4\left(3 \sin \alpha + \frac{5}{2} \cos \alpha + \frac{7}{2}\right)^2}{9(3 + \cos \alpha)^2} \quad (17)$$

A clearer view on how the expansion/packaging ratio changes with the input angle is shown in Fig. 9.

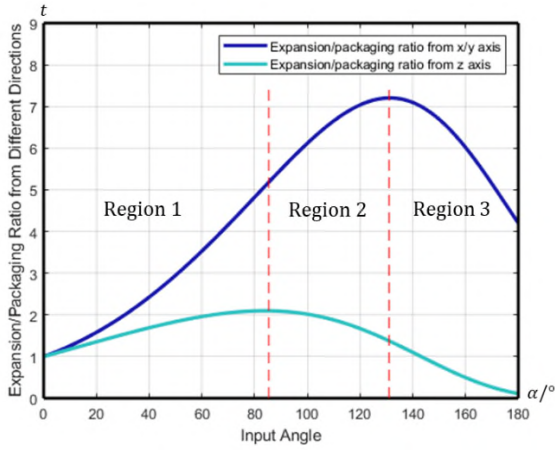


FIGURE 9: Relationship between expansion/packaging ratio t and input angle α from different directions.

It is observed from Fig. 9 that the expansion/packaging ratios reach the local extremum around 0° , 85.37° , 131.2° , and 180° , which divide the graph into three regions. In Region 1 and 3, the structure presents negative Poisson's ratio as the expansion/packaging ratios in different directions have the same tendency when the input angle increases. The basic assembly can work as a modular unit to construct large-scale structures for more configurations, which are suitable for programmable mechanical metamaterials by changing the initial input angle. This will be demonstrated in the section of experiment results.

3. FABRICATION

A single paper sheet can be folded manually with an embossed crease pattern [5] [11] [13]. For polymer films, laser machining can engrave creases or cut a series of holes to produce folding patterns [8, 9]. Unfortunately, neither of the two

fabrication techniques is applicable for the thick-panel origami. For thick panels or blocks, we require flexible but durable hinges to connect them. Appropriate materials and fabrication process should both be taken into consideration.

Additive manufacturing techniques like 3D printing make it a one-step process to create a three-dimensional object by successively adding material layer by layer [14]. With the advances in printing filaments, thermoplastic polyurethane (TPU) material is ready to provide hard and soft segments of different thicknesses. TPU material possesses exceptional mechanical properties including good strength, excellent abrasion, tearing resistance, and advantages on fatigue behaviours [15]. Thus, it is a good choice to work as structures with flexible hinges that can easily be fabricated with a desktop 3D printer (Ultimaker 3 Extended).

In our models, the panels or blocks are rigid whilst their connections are flexible. As the stiffness of TPU material can be changed by thickness, the proposed unfolded waterbomb structure can be seen as thick flat substrates with several thin layers linking them to work as hinges. Because the 3D printer deposits materials layer by layer, the hard parts and soft parts are well connected together. The model for 3D printing is displayed in Fig. 10(a). The finest profile that the 3D printer can achieve is 0.1mm. Thus, to obtain flexibility and durability at the same time, we chose the thickness 0.2mm for soft parts to work as hinges by trial and error. We also found 10mm a suitable thickness for cubes and prisms to ensure their rigidity. In a similar way, we set the width of hinges as 1mm. Using 2.85mm white TPU 95A filament for the printer, we obtain a printed single unit at the stable unfolded state shown in Fig. 10(b). It can achieve all the motions as we have discussed in last section.

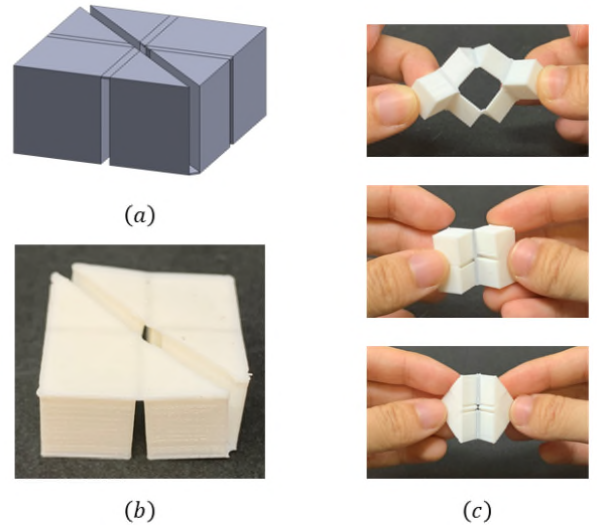


FIGURE 10: Single unit with zero input angles. (a) CAD model for 3D printing; (b) its printing result; (c) folding behaviours of single unit.

With the help of Polyvinyl Alcohol (PVA) as a temporary support material, the model can also be printed at its semi-expanded configurations, which creates structures of different initial states. This method is useful to construct metamaterials of controllable properties by changing their initial input angles. For a single unit, if the input angles are set as 90° , then the waterbomb can be acquired as Fig. 11(a). Hinges should be redesigned to be aligned with new dihedral angles instead of previous cuboid ones, which is shown in Fig. 11(b). The printing result is illustrated in Fig. 11(c), which can remain stable at the semi-expanded state and also reach extreme positions after unfolding, expanding, flipping, and rotating.

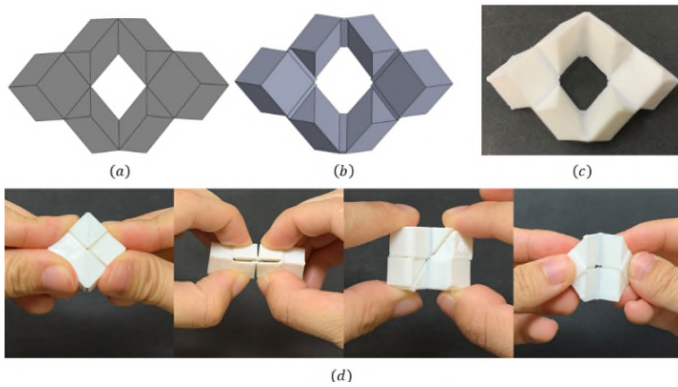


FIGURE 11: Single unit with input angle of 90° . (a) Analytical model; (b) CAD model with new hinges; (c) its printing result where support material has been removed; (d) folding behaviours.

4. EXPERIMENT RESULTS

The fabrication method makes it possible for us to construct tessellations based on a single unit with tiling and pattern techniques. In this section, we will demonstrate the reconfigurability and transformability of a basic modular assembly, large-scale planar and spatial assemblies generated from a single unit.

4.1 Basic Modular Assembly

The basic assembly of four single units can have both individual and synchronic motions, which are validated by using two different printing methods. Model 1 in Fig. 12(a) shows the result of zero initial input angles while Model 2 in Fig. 12(b) shows the one of 90° input angles printed with support. With different initial stable states, the two models exhibit various foldable properties. It is much easier to achieve separate operations on Model 1, and Model 2 is better for synchronic motions. Due to the inbuilt elasticity in the hinges of Model 2, it shows another stable equilibrium state in Fig. 12(c), which can be reached by simply pressing the centre of the model. Both models can work as a module to create large-scale assemblies.

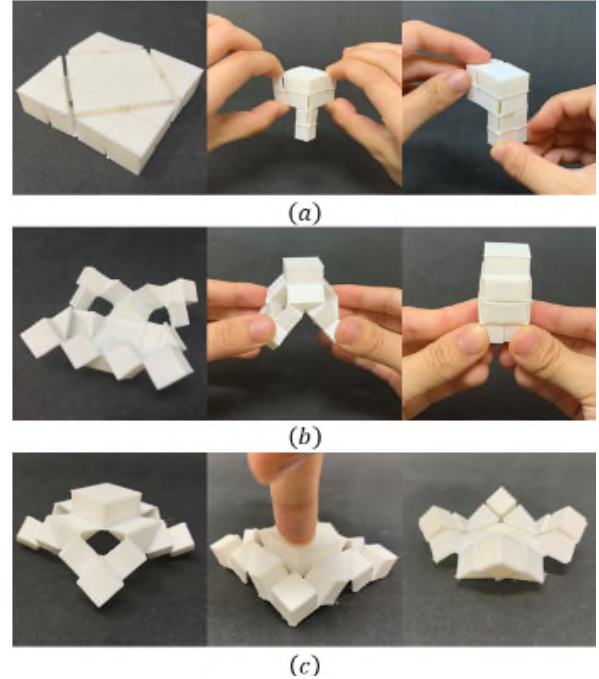


FIGURE 12: Two types of basic assembly and their folding behaviours. (a) Model 1: assembly of zero input angles; (b) Model 2: assembly of 90° input angles; (c) process of changing Model 2 to another stable configuration.

4.2 Planar Assembly

The basic modular assembly can produce a flat panel with grid tiles shown in Fig. 13.

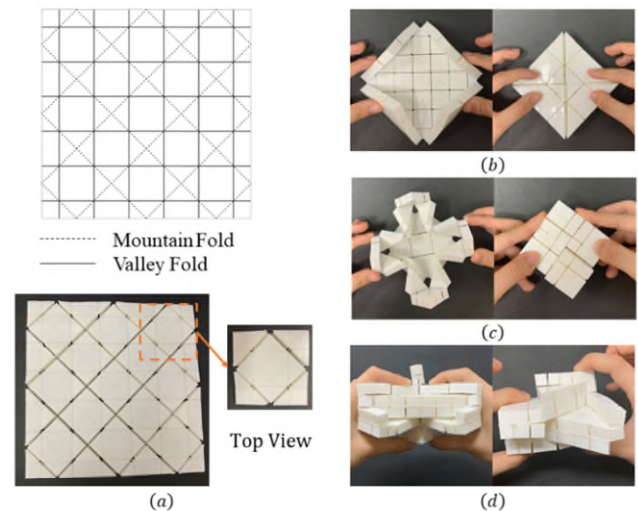


FIGURE 13: 3×3 flat panel from modular assembly. (a) Crease pattern and its 3D printed model; (b) folding the panel into two-layer cuboid; (c) folding the panel into four-layer cuboid; (d) other folding configurations.

As a one-layer flat panel, the structure has high reconfigurability. It can be fully folded into either a two-layer (Fig. 13(a)) or four-layer stack (Fig. 13(c)). Six-layer and eight-layer configurations (Fig. 13(d)) are also reachable by a certain folding sequence. These folding behaviours come from a combination of motions at the bifurcation point.

4.3 Spatial Assembly

The modular assemblies can also be arranged with a shared cube. Then we can create structures that are extendable either planarly or spatially. Examples are shown in Fig. 14 and Fig. 15.

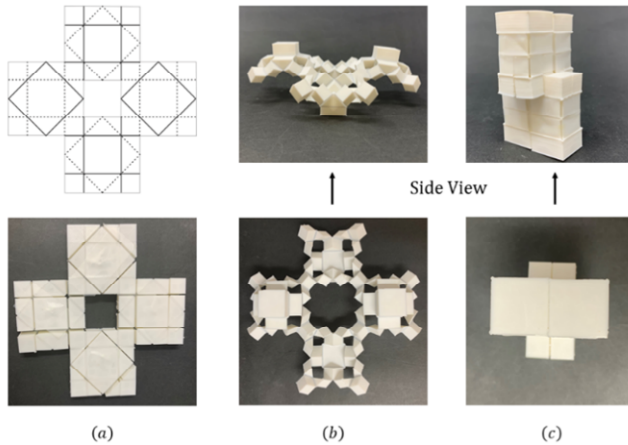


FIGURE 14: Single layer 2×2 spatial assembly. (a) Crease pattern and top view of its printing result; (b) and (c) partially-expanded and fully-folded structures from top and side views.

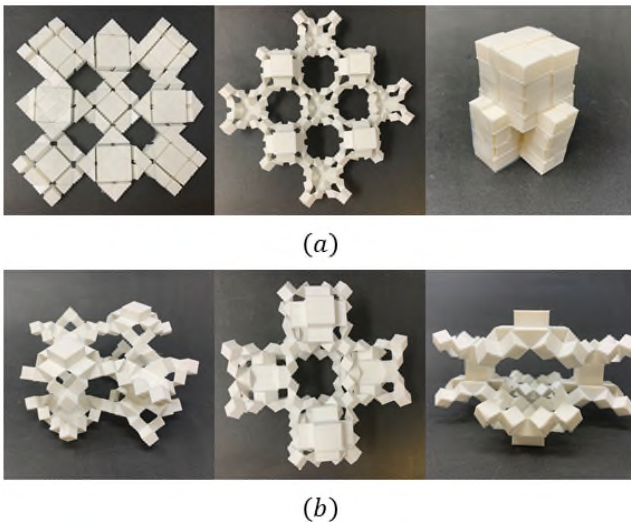


FIGURE 15: Planarly and spatially extended structures. (a) Single layer 3×3 matrix and its folding behaviours; (b) double layer 2×2 spatial structure printed at a semi-expanded state.

All the expansion/packaging ratios of the three spatial structures are the same as the basic modular assembly. Therefore, they keep negative Poisson's ratio with input angles from 0° to 85.37° , and 131.2° to 180° . The concept provides a method to create reconfigurable metamaterials that can be scaled up to any size in the space and tuned for desirable mechanical properties.

5. ROBOTIC CASE STUDY

The folding principles enable the proposed structures to yield compliance. We developed a robotic gripper from the basic assembly as it has circular trajectories on each unit.

Tendon-driven method was chosen to actuate the structure. The basic tendon routes for a single unit are illustrated in Fig. 16. A single unit is defined to have a cube as the fixed base, two connected prisms as active parts and other passive parts. Tendons come through the active prisms and then the base, with one end fixed to the prisms and the other free to be controlled. Each tendon has two states: pulled and loosened. When the control end is pulled, the structure performs the expanding motion. When the tendons are loosened, the structure return to the initial unfolded state due to the elasticity in the hinges.

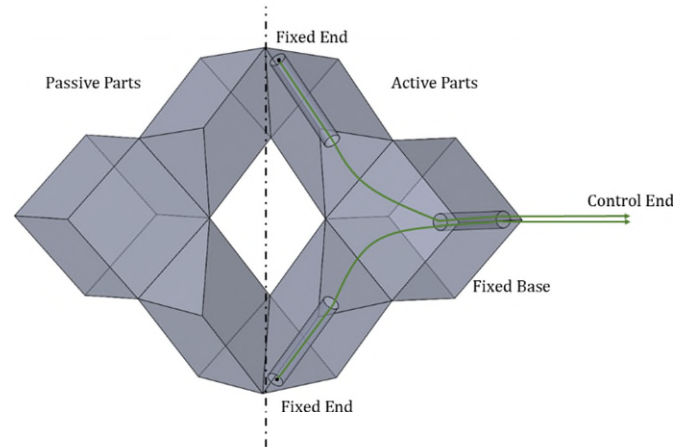


FIGURE 16: Tendon routes to actuate a single unit.

Based on this method, we further designed the structure of a four-finger gripper and its tendon routes as shown in Fig. 17 (a). The gripper weighs $10g$ in total. On its structure, the end of each single unit is regarded as a fingertip, which is rounded to better conform objects. Besides, fishing lines are used as tendons here. The base and two adjacent active parts of each unit are combined, respectively. Thus, tendon paths can also be integrated. Finally, we got four paths instead of eight and one control end to achieve the grasping motion. A semi-expanded model driven by tendons is displayed in Fig. 17(b) and 17(c). All the fingertips are operated synchronically by simply pulling or loosening the control end.

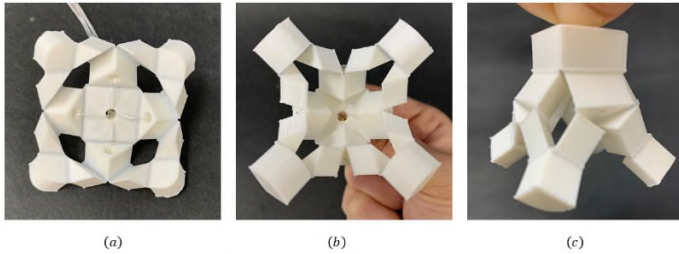


FIGURE 17: Four-finger gripper made from basic assembly. (a) Top view of structure and its tendon routes; (b) and (c) top and side views of semi-expanded structure achieved by pulling tendons to achieve grasping motion.

To control the gripper, we built an electromechanical system based on an Arduino UNO board and a geared motor. The control end is tied on the shaft of the motor, which alters the tendons' state by rotating forward and in reverse.

Next, three objects were used to test the gripper's capability. Grasping motions and objects' properties are shown in Fig. 18, where the gripper shows desirable adaptability and controllability. The circular trajectory of each finger makes it adaptable to objects' shape. As the gripper has only one DOF after the bifurcation point, grasping motion is conducted by simply clicking the control button to pull the tendons.

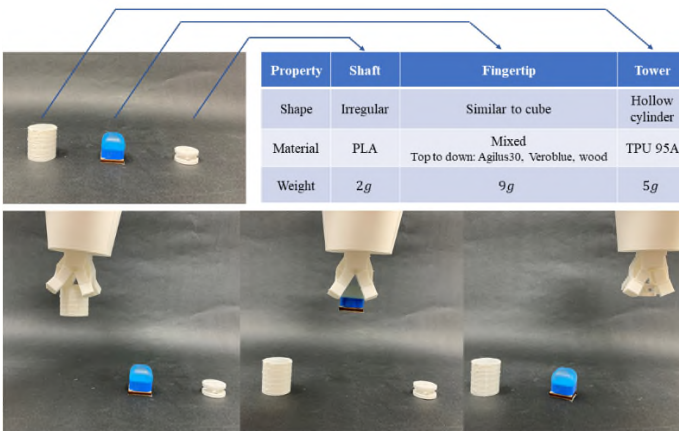


FIGURE 18: Tests of gripper to grasp different objects.

6. CONCLUSIONS AND FUTURE WORK

In this paper, we propose a new structure concept by integrating both rigid and flexible parts for thick-panel origami folding. An additive 3D printing fabrication method is developed to produce hybrid soft-rigid bodies, enabling flexibility and strength at the same time. Along with the mechanism analysis, we start from a single unit based on the six-crease waterbomb pattern and demonstrate its capability to be constructed for modular units, large-scale planar and spatial assemblies. These

structures show desirable reconfigurability for mechanical metamaterials of negative Poisson's ratio. Promising robotic applications are also validated by a four-finger gripper originating from the modular units and actuated by tendon systems.

Future work mainly lies in two areas. One is to further develop robotic applications. For example, the gripper could be obtained in a three-finger form, where separated dexterous manipulation algorithms could be explored in the design. Moreover, morphological computation is also a good way to understand the mechanism of the hybrid soft-rigid bodies to develop soft robotics. Another possibility would be to realize real applications like tuneable metamaterials with wide-range expansion/packaging ratio. In addition to programmability shown in the paper, self-folding ability is also a key factor to consider. Global actuations like electromagnetic materials or shape memory polymers could be implemented to create self-folding hinges.

ACKNOWLEDGMENTS

The authors wish to acknowledge the support of Air Force Office of Scientific Research (FA9550-16-1-0339). Dr. Peter Walters' generous help on 3D printing is much appreciated.

REFERENCES

- [1] Kotikian, Arda., McMahan, Connor., Davidson, Emily. C., Muhammad, Jalilah. M., Weeks, Robert. D., Daraio, Chiara., and Lewis, Jennifer. A. "Untethered soft robotic matter with passive control of shape morphing and propulsion." *Science Robotics* Vol. 4 No. 33 (2019).
- [2] Lv, Ceng., Krishnaraju, Deepakshyam., Konjevod, Goran., Yu, Hongyu., and Jiang, Hanqing. "Origami based Mechanical Metamaterials." *Scientific Reports* Vol. 4 No. 1 (2014).
- [3] Rus, Daniela., and Tolley, Michael. T. "Design, fabrication and control of origami robots." *Nature Reviews Materials* Vol. 3 No. 6 (2018): pp. 101–112.
- [4] Holland, Alexander., and Straub, Jeremy. "Development of origami-style solar panels for use in support of a Mars mission." *Energy Harvesting and Storage: Materials, Devices, and Applications VII* Vol. 9865(2016).
- [5] Jeong, Donghwa., and Lee, Kiju. "Design and analysis of an origami-based three-finger manipulator." *Robotica* Vol. 36 No. 2 (2018): pp. 261–274.
- [6] Chen, Yan., Peng, Rui., and You, Zhong., "Origami of thick panels." *Science* Vol. 349 No. 6246 (2015): pp. 396–400.
- [7] Chen, Y., Feng, Huijuan., Ma, Jiayao., Peng, Rui., and You, Zhong. "Symmetric waterbomb origami." *Proceedings of*

the Royal Society A: Mathematical, Physical and Engineering Sciences Vol. 472 No. 2190 (2016).

- [8] Onal, Cagdas. D., Wood, Robert. J., and Rus, Daniela. “Towards printable robotics: Origami-inspired planar fabrication of three-dimensional mechanisms.” *2011 IEEE International Conference on Robotics and Automation* pp. 4608-4613.
- [9] Onal, Cagdas. D., Wood, Robert. J., and Rus, Daniela. “An Origami-Inspired Approach to Worm Robots.” *IEEE/ASME Transactions on Mechatronics* Vol. 18 No. 2 (2013): pp. 430–438.
- [10] Banerjee, Hritwick., Pusalkar, Neha., and Ren, Hongliang. “Preliminary Design and Performance Test of Tendon-Driven Origami-Inspired Soft Peristaltic Robot.” *2018 IEEE International Conference on Robotics and Biomimetics (ROBIO)* pp. 1214-1219.
- [11] Banerjee, Hritwick., Pusalkar, Neha., and Ren, Hongliang. “Single-Motor Controlled Tendon-Driven Peristaltic Soft Origami Robot.” *Journal of Mechanisms and Robotics* Vol. 10 No. 6 (2018).
- [12] Kamrava, Soroush., Mousanezhad, Davood., Felton, Samuel. M., and Vaziri, A. “Programmable Origami Strings.” *Advanced Materials Technologies* Vol. 3 No. 3 (2018).
- [13] Lee, Dae-Young., Kim, Ji-Suk., Kim, Sa-Reum., Koh, Je-Sung., and Cho, Kyu-Jin. “The Deformable Wheel Robot Using Magic-Ball Origami Structure.” *Proceedings of the ASME Design Engineering Technical Conference* Vol. 6 (2013).
- [14] Shahrubudin, Nurhalida., Lee, Te Chuan., and Ramlan, Rhaizan. “An Overview on 3D Printing Technology: Technological, Materials, and Applications.” *Procedia Manufacturing* Vol. 35 (2019): pp. 1286–1296.
- [15] Wang, Chao., Stiller, Tanja., Hausberger, Andreas., Pinter, Gerald., Grün, Florian., and Schwarz, Thomas. “Correlation of Tribological Behavior and Fatigue Properties of Filled and Unfilled TPUs.” *Lubricant* Vol. 7 No. 7 (2019).